

## PAPER

# Measurement of Disturbances at Telecommunication Ports by Using Both Voltage and Current Probes

Fujio AMEMIYA<sup>†</sup>, Yoshiharu HIROSHIMA<sup>††</sup>, and Nobuo KUWABARA<sup>††</sup>, *Regular Members*

**SUMMARY** Method of measuring disturbances at telecommunication ports has been published by IEC/CISPR. A method using both disturbance voltage and current probes is useful because it does not require any impedance stabilization networks (ISNs). In this paper, the values measured using this method are theoretically and experimentally compared with those measured using ISNs. An experiment using a simple circuit model presents that the value obtained by using this method is lower than that by using ISNs in some cases. A theoretical analysis however derives that the estimated value by adding the margin to the measured value is always guaranteed to be large compared with the value measured by ISNs. The analysis also indicates that the margin is dependent on the deviation of phase angle of ISN and can be calculated by a simple equation. The experiment using actual equipment shows that the estimated results including the margin is always larger than those measured by ISNs. The results of the study show that the method using both disturbance voltage and current probes can be used for measuring the disturbances by taking the margin into account, and this margin can be reduced by improving the phase angle characteristics of the common mode impedance of ISNs.

**key words:** disturbance, telecommunication ports, ISN.

## 1. Introduction

Recent progress in information technologies has accelerated the emergence of various types of telecommunication equipment that uses digital processing circuits. The unwanted emission from the equipment has a potential to disturb the reception of radio waves. Therefore, the International Special Committee on Radio Interference (CISPR) published the limits and methods of measurement of radio disturbance characteristics of information technology equipment (ITE) in 1985 [1]. In Japan, the Voluntary Control Council for Interference by Information Technology Equipment (VCCI) was established in 1985 [2] and has been controlling the emission level of ITE.

Three types of emission have been considered. The first is disturbance through AC power lines, the second is that through space, and the third is that through telecommunication cables. The published specification by the CISPR [1] had no limits for the disturbance through telecommunication cables because the limits and the measurement method were still under-consideration at that time.

The electric field around telecommunication cables

Manuscript received March 21, 2000.

Manuscript revised August 11, 2000.

<sup>†</sup> The author is with NTT Advanced Technology Corporation, Musashino-shi, 180-8585 Japan.

<sup>††</sup> The authors are with NTT Lifestyle and Environmental Technology Laboratories, Musashino-shi, 180-8585 Japan.

generated by the common-mode current on the cable is directly related to the disturbance [3]. The relation between the common-mode voltage at telecommunication ports and the electric field around the cable has been studied [4], [5]. On the other hand, Danffel et al. pointed out that the telecommunication signal has potential to disturb the reception of radio waves [6]. The electromagnetic disturbance concerning with telecommunication systems has been studied [7], [8]. In 1998, the CISPR published CISPR Publication 22 third edition (CISPR 22) [9], which contains the limits and measurement methods for disturbances at telecommunication ports of ITE.

Disturbances at telecommunication ports of ITE are generally measured using an impedance stabilization network (ISN) as specified in CISPR 22 [9]. There are many kinds of telecommunication ports; for example, a private branch exchange (PBX) has several thousand wire terminals and the latest high-speed LAN systems [10] use an 8-wire telecommunication ports, but CISPR 22 only specifies ISNs for 2- and 4-wire ports. A design method of ISNs for measuring the disturbance at telecommunication ports intended to connect more than 6-wires has been studied [11]. On the other hand, high-speed LAN systems [10], [12] are widely used in offices, and these have also potential to disturb the radio wave reception [13]. However, ISNs for measuring the disturbance at telecommunication ports of high-speed LAN systems [10] have not yet been developed.

The CISPR 22 describes four alternative methods in the annex C that should be applied when a suitable ISN is not available. The first method needs coupling and de-coupling networks (CDNs), but CDNs used for high-speed LANs have not been developed. The second method can only be used for ports connected to a shielded cable. It is therefore impossible to apply this method for such systems as high-speed LANs that use unshielded twisted pair (UTP) cable. The third method is the method for measuring both disturbance voltage and disturbance current simultaneously. The fourth method is the method for measuring the common mode impedance before disturbance measurement but this method is still being investigated in CISPR.

The third method can be used to measure disturbances at any kind of ports including high-speed LAN ports because it does not need to use any ISNs. According to the report [14], the disturbance measured by this method are always larger than those measured by ISN. However, this has not yet been confirmed.

In this paper, we investigate the deviations between the measured disturbances using the method described in annex C.1.3 of the CISPR 22 third edition and using an ISN. An equivalent circuit is studied for the measurement set-up of the disturbances. An experiment was carried out using a circuit model derived on the basis of the equivalent circuit. The disturbance levels using both methods are calculated based on the equivalent circuit. An equation to calculate the margin, which means the estimated value by adding the margin to the disturbances level measured by the method of annex C.1.3 is always larger than the level measured by ISNs, is derived from the simulation results. Experiment using actual equipment is described to confirm the theoretical result.

**2. Measurement Method in Annex C.1.3**

The test set-up using the method of measurement described in annex C.1.3 of CISPR 22 (V&I method) is illustrated in Fig. 1. In Fig. 1, A is the measurement point. Both disturbance voltage and disturbance current are measured, and the severest value compared with the relevant disturbance limits is used for the estimation of the test results [14]. Ferrite clamps or similar devices are inserted between the measurement point and the associated equipment (AE) to reduce the deviation of the common-mode impedance when an ISN is used.

The equivalent circuit for the test set-up shown in Fig. 1 is illustrated in Fig. 2. In Fig. 2,  $V$  and  $I$  are disturbance voltage and disturbance current, respectively, and  $V_r$  and  $I_r$  are the disturbance voltage and the disturbance current

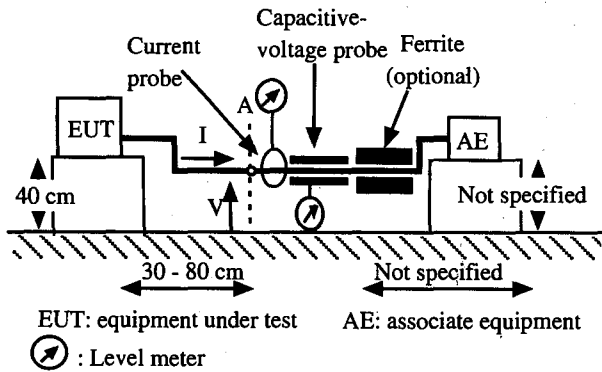


Fig. 1 Test set-up described in annex C.1.3.

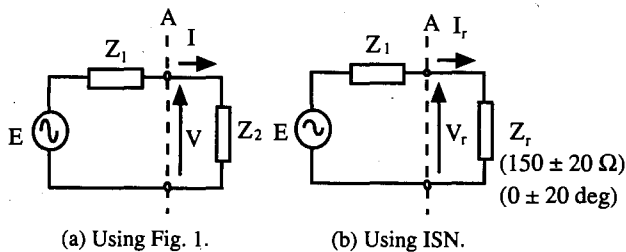


Fig. 2 Equivalent circuit for measuring disturbances at telecommunication ports.

measured by using an ISN. The common-mode impedance  $Z$  is specified in the CISPR 22 [9].  $E$  is a disturbance source,  $Z_1$  is the internal impedance of the disturbance source, and  $Z_2$  is the common mode impedance seeing the AE from the point A in Fig. 1. The effect of the current probe and the capacitive voltage probe are not considered in this circuit because the impedance between the current probe and the cable is less than 25 pF, as described in CISPR 16-1 [15]. The capacitive voltage probe used in this experiment also satisfies this specification.

From the equivalent circuit, the deviations between the measurement results by the V&I method and using an ISN (ISN method) is given by,

$$F_v = V/V_r = \{Z_2(Z_1+Z_r)\}/\{Z_r(Z_1+Z_2)\}, \quad (1)$$

$$F_I = I/I_r = (Z_1+Z_r)/(Z_1+Z_2). \quad (2)$$

Here, we present

$$Z_1 = |Z_1| \cos \theta_1 + j |Z_1| \sin \theta_1, \quad (3)$$

$$Z_2 = |Z_2| \cos \theta_2 + j |Z_2| \sin \theta_2, \quad (4)$$

$$Z_r = |Z_r| \cos \theta_r + j |Z_r| \sin \theta_r, \quad (5)$$

Substituting Eqs. (3), (4), (5) into Eq. (2), we get

$$|F_I| = \sqrt{\frac{|Z_1|^2 + |Z_r|^2 + 2|Z_1||Z_r|\cos(\theta_1 - \theta_r)}{|Z_1|^2 + |Z_2|^2 + 2|Z_1||Z_2|\cos(\theta_1 - \theta_2)}} \quad (6)$$

From Eq. (1),

$$|F_v| = \{|Z_2|/|Z_r|\}|F_I|. \quad (7)$$

The larger the deviations from  $V_r$  or  $I_r$ , the severer the measured value to the specified value. Thus, the test results are given by

$$F_r = \begin{cases} |F_v| & (|F_v| > |F_I|) \\ |F_I| & (|F_I| > |F_v|) \end{cases} \quad (8)$$

In the case of that  $Z_1$ ,  $Z_2$  and  $Z_r$  are presented by pure resistance, this means  $\theta_1 = \theta_2 = \theta_r = 0$ . In this case Eqs. (6) and (7) are then given by the following equations.

$$|F_I| = \{1 + |Z_r|/|Z_1|\} / \{1 + |Z_2|/|Z_1|\} \quad (9)$$

$$|F_v| = \{1 + |Z_1|/|Z_r|\} / \{1 + |Z_1|/|Z_2|\} \quad (10)$$

In Eq. (9), when  $|F_I| < 1$ , we get

$$\{|Z_r|/|Z_1|\} < \{|Z_2|/|Z_1|\}. \quad (11)$$

From Eq. (11), we get

$$\{|Z_1|/|Z_r|\} > \{|Z_1|/|Z_2|\}. \quad (12)$$

Substituting Eq. (12) into Eq. (10), we get

$$|F_v| > 1. \quad (13)$$

Using Eq. (8), we get

$$F_i > 1 \tag{14}$$

Using the same procedure, when  $|F_v| < 1$ , we get

$$|F_i| < 1. \tag{15}$$

and

$$F_i > 1 \tag{16}$$

This means that the measured value by the V&I method is always larger than that by the ISN method when  $Z_1, Z_2$ , and  $Z_r$  are the pure resistance. However, these are not the pure resistances usually. The amplitude of  $Z_1$  and  $Z_2$  can change from 0 to an infinite value and these phase angels can change from  $-\pi/2$  to  $\pi/2$ . The amplitude of  $Z_r$  can change from 130  $\Omega$  to 170  $\Omega$  and its phase angle can change from  $(-1/9)\pi$  to  $(1/9)\pi$  according to the specification [9]. These changes are occurred independently. In such conditions, we should confirm whether  $F_i$  is always more than 1 or not. This paper investigates it theoretically and experimentally.

### 3. Experiment

An experiment was carried out to confirm this theory using electric circuit model obtained from the equivalent circuit shown in Fig. 2. The experimental set-up is shown in Fig. 3. The voltage source in Fig. 2 was constructed to terminate the input signal by a low resistance  $R_s$ . The resistance  $R_r$  of 150  $\Omega$  means the common mode impedance of ISN. The  $R_1, C_1, R_2, C_2$  values determine that  $|Z_1|$  and  $|Z_2|$  are 150  $\Omega$  at a frequency from 0.15 to 30 MHz. The disturbance current  $I$  and the disturbance voltage  $V$  were measured by a current probe and a high impedance probe whose input impedance is 1 M $\Omega$ , respectively. The transmission loss between signal source output port and the output port of these probes was measured using a network analyzer. The  $F_i$  value is obtained using Eq. (6) in the case of that  $|F_v|$  and  $|F_i|$  are given by the following equation.

$$|F_v| = L_v/L_{vr}, \quad |F_i| = L_i/L_{ir} \tag{17}$$

where,  $L_v$  is the transmission loss measured by the voltage probe when the point A is terminated by  $R_2+1/(j\omega C_2)$ ,  $L_{vr}$  is the transmission loss when the point A is terminated by  $R_r, L_i$

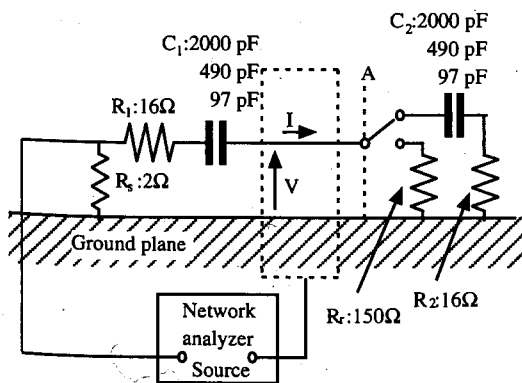


Fig. 3 Experimental set-up to measure the conversion factor.

is the transmission loss measured by current probe when the point A is terminated by  $R_2+1/(j\omega C_2)$ , and  $L_{ir}$  is the transmission loss when the point A is terminated by  $R_r$ . The theoretical value is calculated using Eq. (8).

The investigation results are shown in Fig. 4. In Fig. 4, the solid lines are the calculated values and the dots are measured values. The measured values clearly agree with the calculated values and the  $F_i$  becomes less than 0 dB when the frequency changes from 0.1 to 30 MHz. This means that the impedances of  $Z_1$  and  $Z_2$  change according with frequency change and, the conditions when  $F_i$  is less than 1 are satisfied at some frequencies.

Since CISPR 22 specified to measure disturbances from 0.15 MHz to 30 MHz, the possibility of the  $F_i$  value being less than 1 is not so small.

### 4. Calculation of Margine

The experimental result in Sect. 3 shows that the measured value by the V&I method is smaller than that by the ISN method in same cases. We should obtain a value to guarantee that the measured value by the V&I method is always larger than that by the ISN method. We call the value as margin in this paper. This is the difference between the values obtained by the V&I and the ISN methods. This is the special specification which is substituted for the formal specification and is used at test laboratories to guarantee that the equipment satisfying the specification at a test laboratory also satisfies the specification at other test laboratories.

When  $|F_v| > |F_i|$ , from Eqs. (1) and (8), we get

$$\begin{aligned} V'(\text{dB}\mu\text{V}) &= V(\text{dB}\mu\text{V}) + F_{im}(\text{dB}) \\ &= V(\text{dB}\mu\text{V}) - 20\log(F_{i\min}) \\ &= 20\log(|F_v|) + V_r(\text{dB}\mu\text{V}) - 20\log(F_{i\min}) \\ &= 20\log(F_v) + V_r(\text{dB}\mu\text{V}) - 20\log(F_{i\min}) \\ &= \{20\log(F_v) - 20\log(F_{i\min})\} + V_r(\text{dB}\mu\text{V}) \end{aligned} \tag{18}$$

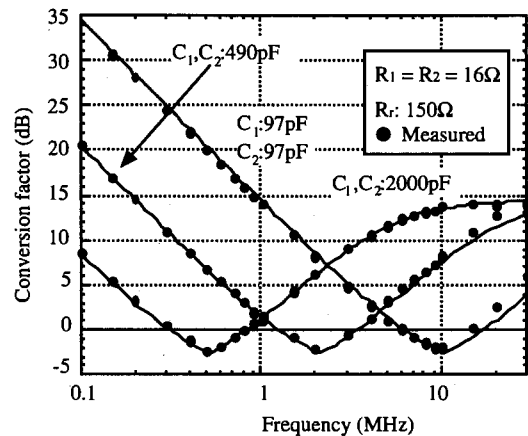


Fig. 4 Measurement results of the conversion factor.

where,  $F_m$  is the margin and  $F_{\min}$  means the minimum value of  $F_r$ . Then

$$\{20\log(F_r) - 20\log(F_{\min})\} \geq 0 \quad (19)$$

In Eq. (19), we get

$$V'(\text{dB}\mu\text{V}) \geq V_r(\text{dB}\mu\text{V}). \quad (20)$$

When  $|F_v| < |F_r|$ , using the same procedure, we get

$$I'(\text{dB}\mu\text{V}) \geq I_r(\text{dB}\mu\text{V}) \quad (21)$$

Equations (18) to (21) show that the measured value by the V&I method is always larger than that by the ISN method when we use the margin.

As shown in Eq. (18), the margin is the minimum value of  $F_r$ ,  $F_{\min}$ . In this section, we show how to determine  $F_{\min}$ .

There are six parameters as shown in Eqs. (6) and (7). Here, we set

$$a = |Z_1| / |Z_r|, \quad (22)$$

$$b = |Z_2| / |Z_r|, \quad (23)$$

$$c = \theta_1 - \theta_2, \quad (24)$$

$$d = \theta_1 - \theta_r. \quad (25)$$

Substituting Eqs. (22) to (25) into Eqs. (6) and (7), we get

$$|F_r| = \sqrt{\frac{a^2 + 1 + 2a \cos(d)}{a^2 + b^2 + 2ab \cos(c)}} \quad (26)$$

$$|F_v| = b|F_r|. \quad (27)$$

Then, the parameters are reduced from six to four. These parameters change independently with each other. So, when we calculate the dependence of one parameter, the other parameters are considered as constants.

It is difficult to calculate the  $F_r$  value analytically because the calculation results change by the values of  $|F_r|$  and  $|F_v|$  shown in Eqs. (8), (26), and (27). First, we investigate the conditions, when  $F_r$  has the minimum value, by theory and simulation.

The range of the parameters  $Z_1$ ,  $Z_2$ , and  $Z_r$  for simulation is shown in Table 1. The amplitude of  $Z_1$  and  $Z_2$

Table 1 Calculation parameters.

Parameters	Range	Parameters	Range
$ Z_1 $	1 - 10,000	$\arg(Z_1)$	$-\pi/2 - \pi/2$
$ Z_2 $	1 - 10,000	$\arg(Z_2)$	$-\pi/2 - \pi/2$
$ Z_r $	130 - 170	$\arg(Z_r)$	$-\pi/9 - \pi/9$
$\log(a)$	-3 - 3 (step: $\log(1000)/50$ )		
$\log(b)$	-3 - 3 (step: $\log(1000)/50$ )		
$c$	$-\pi - \pi$ (step: $\pi/90$ )		
$d$	$-(11/18)\pi - (11/18)\pi$ (step: $\pi/90$ )		

changes from 1 to 10,000 as for the typical range. The angles of  $Z_1$ ,  $Z_2$  change all range and the amplitude and angle of  $Z_r$  change in the allowable range [9].

From Eqs. (22) to (25) and Table 1, the range of  $a$ ,  $b$ ,  $c$ , and  $d$  are calculated, and the range listed in Table 1 is determined to contain these calculated range. Table 1 also shows the step sizes of  $\log(a)$ ,  $\log(b)$ ,  $c$ , and  $d$  value for calculation. They are determined to get a sufficient accuracy.

#### 4.1 Dependence of $c$ Value

We consider that  $c$  value is variable. In Eqs. (26) and (27),  $a > 0$ ,  $b > 0$ ,  $1 \geq \cos(c) \geq -1$ , and  $1 \geq \cos(d) \geq -0.342$ .  $|F_r|$  in Eq. (26) and  $|F_v|$  in Eq. (27) have the minimum value when  $\cos(c) = 1$  because  $\cos(c)$  exists only the denominator of Eq. (26). A calculation example is shown in Fig. 5. In this figure, horizontal axis is  $c$  value and vertical axis is  $F_r$  value in dB normalized by the minimum value of  $F_r$  for each parameter. In the calculation,  $a$  of 1,  $b$  of 1, 10, 100, and  $d$  of  $\pi/2$  are used as calculation parameters. Figure 5 shows that the  $F_r$  has the minimum value for  $b$  of 1, 10, 100 when  $c$  is 0 ( $\cos(c) = 1$ ). This result expects that  $F_r$  has the minimum value for any  $a$ ,  $b$ , and  $d$  value when  $c$  is 0.

Figure 6 shows the  $c$  value when  $F_r$  has the minimum value. Here,  $a$ ,  $b$ ,  $c$  and  $d$  change in the range shown in Table 1. The step sizes for calculation are selected from the values shown in Table 1. The vertical axis in Fig. 6 is the  $F_{\min}$  value for each  $a$ ,  $b$ ,  $d$  value. Figure 6 shows that  $F_r$  has the minimum value for any  $a$ ,  $b$ , and  $d$  value when  $c$  is 0. Then  $F_{\min}$  is given by

$$F_{\min}(a, b, c, d) = F_{\min}(a, b, 0, d). \quad (28)$$

#### 4.2 Dependence of $d$ Value

When  $c$  is 0, Eqs. (26) and (27) are given by

$$|F_r| = \frac{a^2 + 1 + 2a \cos(d)}{a^2 + b^2 + 2ab}, \quad (29)$$

$$|F_v| = \sqrt{\frac{\{a^2 + 1 + 2a \cos(d)\}}{\{(a/b)^2 + 1 + 2(a/b)\}}} \quad (30)$$

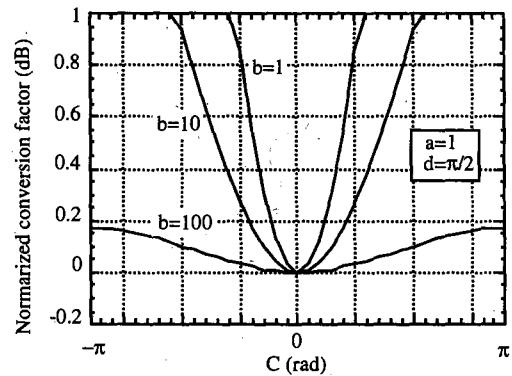


Fig. 5 Calculation example of normalized conversion factor.

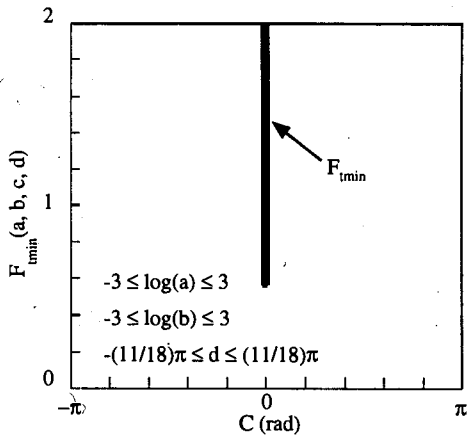


Fig. 6 c value when  $F_c$  is the minimum value.

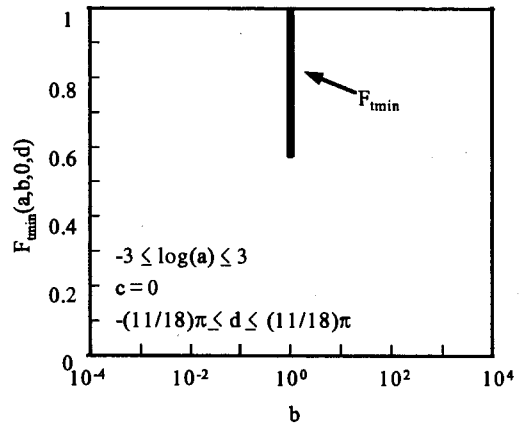


Fig. 8 b value when  $F_c$  is the minimum value.

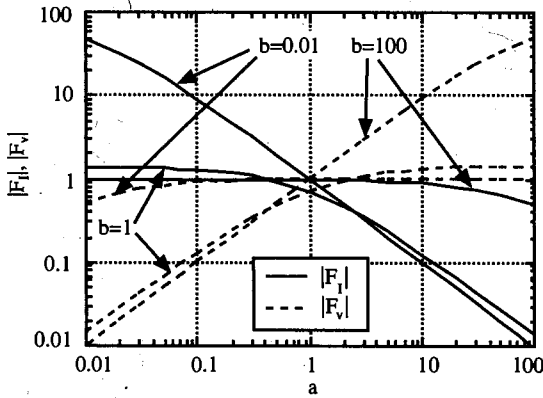


Fig. 7 Calculation example of  $|F_h|$  and  $|F_v|$ .

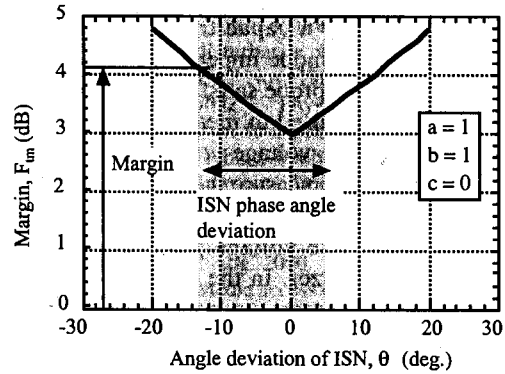


Fig. 9 The minimum value of conversion factor when the angle of an ISN common-mode impedance changes.

From Eq. (29),  $|F_h|$  simply decreases when  $b$  increases because  $a > 0$  and  $b > 0$ . On the other hand, from Eq. (30),  $|F_v|$  simply increases in proportion to  $b$  value. A calculation example of  $|F_h|$  and  $|F_v|$  is shown in Fig. 7. In Fig. 7, horizontal axis is  $b$  value, and vertical axis is  $|F_h|$  and  $|F_v|$ . As shown in Fig. 7,  $|F_h|$  simply decreases when  $b$  increases and  $|F_v|$  simply increases in proportion to  $b$  value. This results expect  $F_{min}(a,b,0,d)$  has the minimum value when  $|F_h|$  equal to  $|F_v|$  ( $b = 1$ ) because  $F_c$  is the larger value of  $|F_h|$  and  $|F_v|$ .

Figure 8 shows the  $b$  value when  $F_{min}(a,b,0,d)$  is the minimum. Here,  $a$ ,  $b$ , and  $d$  change in the range shown in Table 1. The step sizes for calculation are selected from the values shown in Table 1. The vertical axis in Fig. 8 is the  $F_{min}$  value for each  $a$  and  $d$  value. Figure 8 shows that  $F_c$  has the minimum value for any  $a$  and  $d$  value when  $b$  is 1. Therefore,  $F_{min}(a,b,0,d)$  is given by

$$\begin{aligned}
 F_{min}(a,b,c,d) &= F_{min}(a,1,0,d) \\
 &= F_{min}(a,1,0,d) \\
 &= F_{min}(a,1,0,d) \\
 &= \sqrt{\frac{\{a^2 + 1 + 2a\cos(d)\}}{\{a^2 + 1 + 2a\}}}
 \end{aligned}$$

$$= \sqrt{1 - 2\{1 - \cos(d)\} / F_a(a)} \tag{31}$$

where

$$F_a(a) = a + (1/a) + 2 \tag{32}$$

In Eq. (31),

$$\{1 - \cos(d)\} \geq 0. \tag{33}$$

Then, when  $F_a(a)$  is the minimum,  $F_{min}(a,1,0,d)$  is the minimum. The value of  $a$ , when  $F_a(a)$  is the minimum, is obtained as follows;

$$dF_a(a)/da = (1 - 1/a^2) = 0. \tag{34}$$

From  $a > 0$ ,  $a$  of 1 is obtained. Then,

$$\begin{aligned}
 F_{min}(a,b,c,d) &= F_{min}(1,1,0,d) \\
 &= \sqrt{0.5 + \cos(d)} / 2 \tag{35}
 \end{aligned}$$

From Eq. (35),  $d$  value of  $-(11/18)\pi$  or  $(11/18)\pi$  is obtained when  $F_{min}(a,b,c,d)$  is the minimum. From Table 1 and Eq. (25),  $d$  of  $-(11/18)\pi$  means that  $\theta_r$  is  $-(1/9)\pi$  and  $\theta_l$  is  $-\pi/2$ , while  $d$  of  $(11/18)\pi$  means that  $\theta_r$  is  $(1/9)\pi$  and  $\theta_l$  is  $\pi/2$ . This means that  $F_{min}(a,b,c,d)$  is the minimum when  $\theta_l$  is  $\pi/2$  or  $-\pi/2$ . Then, from Eq. (18), the margin  $F_m$  is given by

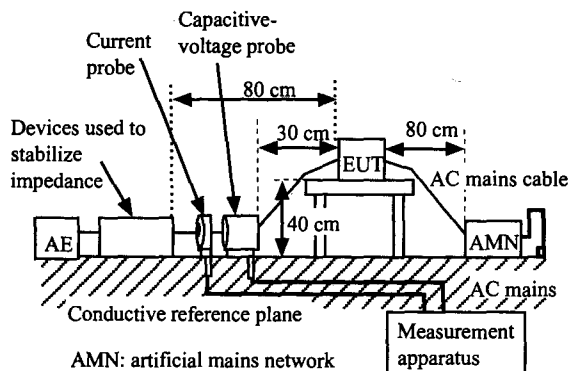
$$F_m(\theta_r) = -20\log_{10}\sqrt{(1 - |\sin\theta_r|)} / 2 \tag{36}$$

Figure 9 shows the calculation results of  $F_{im}$ . The vertical axis is the  $F_{im}$  and the horizontal axis is  $\theta_r$  that is the phase angle of the common mode impedance of ISN. From Fig. 9, the  $F_{im}$  is the minimum when  $\theta_r$  is 0 and increases in proportion to the absolute value of the phase angle. The  $F_{im}$  of 4.8 dB is obtained when  $\theta_r$  is  $-\pi/9$  or  $\pi/9$  that is the maximum allowable phase angle specified in the CISPR 22 [9]. The  $F_{im}$  can be reduced by using an ISN whose maximum phase angle is lower than that specified in the CISPR 22, as shown in Fig. 9.

**5. Measurement Example**

The set-up used for measuring disturbances is illustrated in Fig. 10. Telecommunications equipment was used as the equipment under test (EUT). A 4-wire telecommunications line was used to connect the EUT to the AE. An ISN, an absorbing clamp, and a capacitive clamp were used to stabilize the common-mode impedance between the wires and ground. A current probe satisfying the requirements in CISPR 16-1 [15] was used to measure the common mode current. The capacitive-voltage probe with an electrostatic shield [16] was used to measure the common mode voltage, and it was placed 30 cm away from the EUT. The conversion factor of the capacitive-voltage probe was measured by using a network analyzer. In the measurement, the same cable used in the experiment was connected to the probe and was terminated by 50  $\Omega$ . The disturbance value  $V_r$  was also measured using an ISN for reference. The values subtracting 44 dB from  $V_r$  are used as the reference  $I_r$  for the measurement using a current probe. The absorbing clamp, the capacitive clamp, and an ISN, which are used to stabilize the common-mode impedance, are inserted between the voltage probe and AE to investigate the effect of the common-mode impedance stabilization.

The measurement results are shown in Fig. 11(a). In this figure, the vertical axis is the deviations, which are the larger values of  $V/V_r$  or  $I/I_r$  for each frequency. The measured value, when the ISN was used for impedance stabilization, is almost the same as the reference values. This



**Fig. 10** Experimental set-up used to measure disturbances at telecommunication ports using both current probe and capacitive-voltage probe.

means that the measured result by the V&I method well agrees with the results by the ISN method when the common-mode impedance is the same value of the ISN.

The measured values without using an ISN for impedance stabilization are different from the values measured by using the ISN in most of the measured frequency points, and the maximum deviation was more than 20 dB at 0.2 MHz. The values without using the ISN for impedance stabilization are less than those by the ISN method at around 6 MHz. Therefore, the margin described in Sect. 4 is needed to guarantee that the measured values by the V&I method are always larger than those by ISN method.

Figure 11(b) shows that the measurement results  $V'$  or  $I'$  using Eq. (18). The  $\theta_r$  of seven degrees, which is the maximum absolute phase angle of the ISN in the experiment, is used for the calculation of the  $F_{im}$ . All the measured values are above 0 dB. The result shows that the disturbances can be measured by the V&I method taking

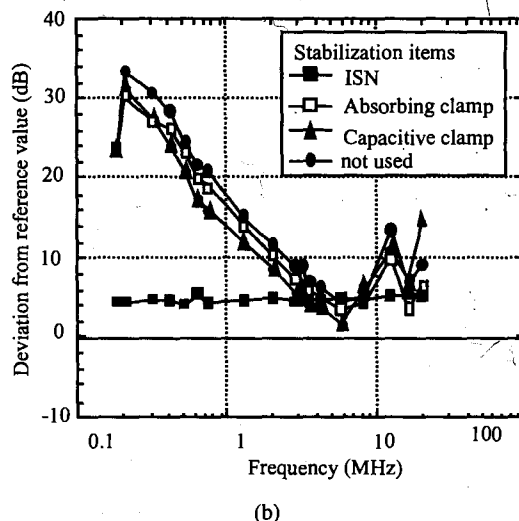
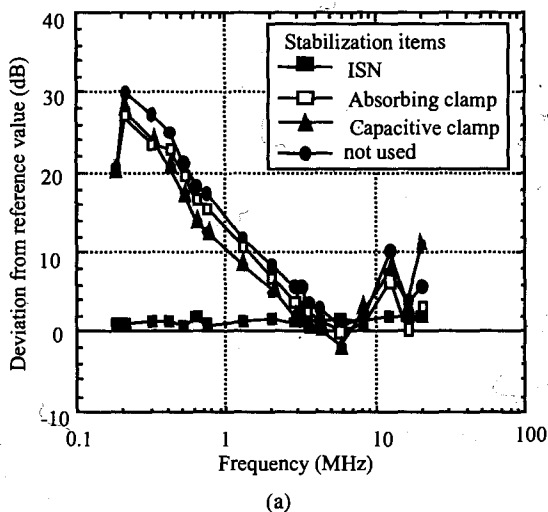


**Fig. 11** (a) Measured deviation from reference value. (b) Measured deviation from reference value taking into account of the margin.